Nanoscale

Accepted Manuscript

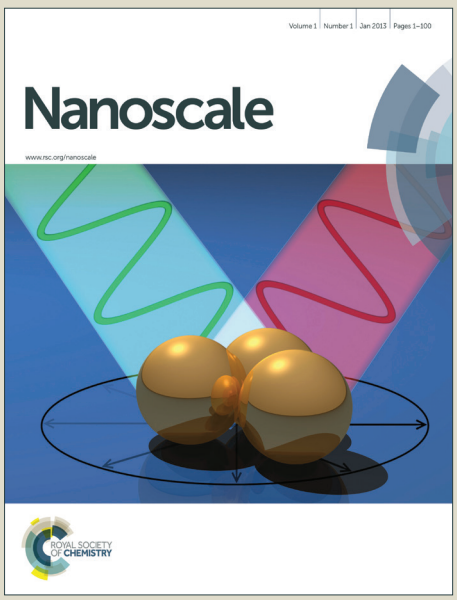

ROYAL SOCIETY OF CHEMISTRY

www.rsc.org/nanoscale

Tuning Non-Doped Carbon Nanotubes to an Efficient Metal-Free Electrocatalyst for Oxygen Reduction Reaction by Localizing the Orbital of Nanotubes with Topological Defects

Shujuan Jiang,[a] Zhe Li, *[b] Huayu Wang,[c] Yun Wang,[a] Lina Meng,[a] and Shaoqing Song*[a]

[a] *Key Laboratory of Radioactive Geology and Exploration Technology Fundamental Science for National Defense, School of Chemistry, Biology and Materials Science, East China Institute of Technology, Nanchang, Jiangxi Province 330013, P. R. China.*

[b] *Key Laboratory of Catalysis and Materials Science of the State Ethnic Affairs Commission &Ministry of Education, South-Central University for Nationalities, Wuhan, Hubei Province, 430074, P. R. China.*

[c] *Jiangxi University of Traditional Chinese Medicine, Nanchang, Jiangxi Province 330013, P. R. China.*

Table of Contents

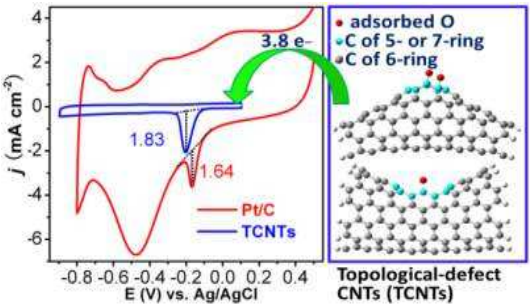

Non-doped CNTs were tuned to be an efficient ORR electrocatalyst by introducing topological defects to localize the orbital of CNTs, which enables the enhancement of O_2 chemisorption and the electrocatalytic activity.

Abstract

Breaking the electron delocalization of sp^2 carbon materials by heteroatom doping is a practical strategy to produce metal-free electrocatalysts of oxygen reduction reaction (ORR) for fuel cells. Whether carbon nanotubes (CNTs) can be efficiently tuned into ORR electrocatalysts only by intrinsic defects rather than heteroatom doping has not been well studied yet in experiment and theory. Here we introduce topological defects of non-hexagon carbon rings into CNTs to break the delocalization of their orbitals, and make such type of CNTs to be a high-performance ORR catalyst. The electrochemical tests and theoretical study indicate that the O_2 chemisorption and the following electrocatalytic activity are promoted by the introduced topological defects and show a strong dependence on the defect amount. Such topological-defect CNTs (TCNTs) have an excellent ORR performance owing a 3.8-electron-transferring process, ~4 times higher current density and ~120 mV more positive peak potential than normally straight CNTs. Moreover, TCNTs show a higher steady-state diffusion current density and much better stability and immunity to crossover effect as compared with commercial Pt/C catalyst. Hence, our results strongly suggest that tuning the surface structure of CNTs with non-hexagon carbon rings is a novel strategy for designing advanced ORR electrocatalysts for fuel cells.

1. Introduction

The oxygen reduction reaction (ORR) commonly catalysed by the Pt-based electrocatalyst is one of the most crucial processes limiting the electrochemical energy conversion in fuel cells[1,2]. Its sluggish electron-transfer kinetics requires high Pt loading to ensure the efficient operation of the reaction system. Hence, the large-scale application of fuel cell is hampered by the very limited reserves, high cost and inactivation by CO poisoning.[3,4] To resolve this bottleneck, great efforts have been devoted to exploring the advanced ORR catalysts to rival the commercial Pt/C catalyst in activity and durability by reducing Pt loading with alloying or structural regulation,[5-12] non-Pt metals,[13-20] or even metal-free species electrocatalysts.[21-43]

The sp^2-hybridized carbon materials have abundant free-flowing π electrons, which make them potentially activate towards some reactions needing electrons, such as ORR. However, to become an electrocatalysts for ORR, the inert π electrons in delocalization state need to be activated. For example, doping carbon nanostructures with electron-rich nitrogen could transform them into promising metal-free electrocatalysts for ORR.[25-28,33,35] It has been revealed that the delocalization of π electrons can be broken by conjugating π electrons with the lone-pair electrons donated by N dopants, thus O_2 molecules can be reduced on those positively charged C atoms connected to N.[25] In our recent work, it is revealed that for electron-deficient B-doped carbon nanotubes (BCNTs), the delocalized π electrons can also be disturbed and activated for catalysing ORR by the conjugation between the vacant $2p_z$ orbital of B and the π system of C.[40] According to the experimental results and theoretical calculations, we have summarized two key factors to transform sp^2 carbon into metal-free ORR electrocatalysts by doping: (1) breaking the delocalization orbitals of sp^2 carbon to create charged sites favorable for O_2 adsorption regardless of the electron-rich (N) or electron-deficient (B) dopant; and (2) activating the

adjacent carbon π electrons for O_2 reduction. Based on these progresses, introducing electron-rich and/or electron-deficient structures into CNTs should be a general route to prepare carbon-based metal-free ORR electrocatalysts.

It is known that carbon nanotubes are composed entirely of sp^2-bonded carbon atoms in a hexagonal network and shown a smooth straight topography.[44] Relative to the carbon hexagon structures, non-hexagon (e.g., pentagon, heptagon and octagon) structures introduced in CNTs are considered as topological defects,[45-47] which can bring a twisted morphology due to the changed C-C bond length in the original orderly graphitic lattice.[48] For example, the introduction of pentagons to CNTs will produce a convex structure because of the longer C-C bond in pentagon carbon rings, in contrast, heptagon or octagon gives a concave structure that results from the shorter C-C bond.[49,50] It was predicted in theory, that a pentagon will induce acceptor-like electronic states near the valence band, while a heptagon will induce donor-like electronic states around the conduction band.[51,52] Intuitively, introducing topological defects into CNTs would disturb the evenly distribution of the delocalized orbitals of hexagon-carbon materials, finally enable them to be an ORR catalyst. In this study, topological-defect CNTs (TCNTs) were facilely synthesized with ethanol as precursor. The experimental and theoretical studies reveal that topological defects can break the inertness of CNTs and turn CNTs into excellent ORR electrocatalysts. Electrochemical measurements show that, with increasing topological defect density, the onset and peak potentials for ORR on CNTs shift positively and the current density increases significantly, indicating a strong dependence of the ORR performance on topological defect amount. These results demonstrate that, simply activating their π electrons by introducing non-hexagon sp^2 carbon ring without using hazardous and poisonous heteroatom precursors,

such as ammonia and organic boron, CNTs can be designed and optimized to be an advanced metal-free ORR electrocatalyst.

2. Experimental section

Preparation of CNT samples

TCNTs were facilely synthesized at 650~850 ^{o}C by CVD method with environment-friendly ethanol as precursor. The bimetallic Fe-Co supported on γ-Al_2O_3 as catalyst was obtained as follows: 1.0 mmol $Fe(NO_3)_3$ and 2.0 mmol $Co(NO_3)_3$ were dissolved to 10 mL aqueous solution, and then this mixed solution was dropped into 1g γ-Al_2O_3 until a paste-like mixture was obtained. After dried at room temperature, the mixture was dehydrogenated at 450 ^{o}C in air for 5 h calcination. The obtained solid block was grinded into powder of 60 mesh, and denoted as Fe-Co/γ-Al_2O_3. TCNTs were prepared as follows: 20 mg Fe-Co/γ-Al_2O_3 catalyst powder was placed in the central part of a horizontal quartz tube in the furnace. After the reaction chamber was evacuated and flushed with N_2 for three times to remove oxygen and moisture, the reactor was heated to the reaction temperature at a rate of 10 °C min^{-1} in N_2. 2 mL ethanol was then introduced into the reaction zone by an injection pump and the flowing Ar of 1400 sccm in 20 min. After that, the reactor was cooled in N_2 and the dark spongelike product was obtained and denoted as TCNTs-1, TCNTs-2 and TCNTs-3 corresponding to the three preparation temperatures of 650, 750 and 850 °C. For comparison, CNTs were synthesized at the same temperatures with benzene as precursor and denoted as CNTs-1, CNTs-2 and CNTs-3, respectively. All CNT samples were refluxed in 6 M NaOH and 6M HCl aqueous solution at 110 ^{o}C for 4 h in turn to remove the Al_2O_3 support and metal catalysts, respectively. The purified CNTs were thoroughly washed with distilled water until the pH value of the filtrate reached 7, and then dried at 70 ^{o}C overnight for further study.

Characterization

Transmission electron microscopy (TEM) (JEOL-JEM-1005 at 100 kV), high-resolution TEM (HRTEM) (JEM2010 at 200 kV), and Raman spectroscopy (Renishaw inVia Raman Microscope with an argon-ion laser at an excitation wavelength of 514 nm) were used to characterize the products.

Electrochemical measurements

Electrochemical measurements including cyclic voltammetry (CV), rotating disk electrode (RDE) and rotating ring-disk electrode (RRDE) voltammetries were carried out at 25 ^{o}C with a CHI 760C workstation (CH Instruments). Ag/AgCl and Pt wire served as reference and counter electrodes, respectively. CV and RDE voltammetry were collected with a glassy carbon (GC) electrode (3 and 5 mm diameter, respectively), and RRDE voltammetry were performed on a GC disk electrode (5 mm diameter) surrounded by a Pt ring (6.5 mm inside diameter). The GC electrode was modified as following. Simply, 1 mg sample was dispersed into 1 mL mixture of water, ethanol and Nafion (DuPont, 5 wt%) with the volume ratio of 1 : 3.85 : 0.15 by ultrasonication and a suspension with a concentration of 1.0 mg mL^{-1} was obtained. Then 20 μL of this ink was dropped onto the GC disk intermittently and dried thoroughly in air for 12 hours. ORR evaluation was performed in 0.1 M NaOH electrolyte saturated and protected by O_2. For comparison, commercial Pt/C (20 wt% Pt loading, Johnson Matthey) catalyst was also used in the electrochemical tests. O_2-stripping experiments were conducted in 0.1 M NaOH solution which was purged with nitrogen for 30 min and then bubbled with O_2 gas (99.99%) for 45 min for O_2 adsorption on catalysts. The residual O_2 in the solution was subsequently removed by N_2 purging for 60 min. The O_2-stripping CV curves were recorded at a scan rate of 5 mV s^{-1}. The 40000 s steady-state chronoamperometric response was tested at the polarizing potential of -0.3

V in the O_2-saturated electrolyte by bubbling O_2 into the electrolyte with a flow of 30 sccm. At 1200 or 520 s in the steady-state chronoamperometric tests, 1.0 mL methanol or 30 sccm flow of CO (or N_2) was introduced into the electrolyte to examine the methanol crossover.

Computational Details

DFT calculation was performed on armchair (5,5) single-walled CNT model (CNT(5,5)) and CNT(5,5) with pentagon/heptagon structures (PCNT(5,5)/HCNT(5,5)). Metallic armchair (5,5) single-walled CNT with length of 5 unit cells and diameter of 6.85 Å was used in the theoretical calculations. The terminal sites of the nanotubes were saturated with hydrogen atoms in order to avoid the edge effect. Theoretical calculations based on DFT were carried out with Gaussian09 package.[53] The geometrical optimizations were performed using DFT method with Becke's hybrid three parameter nonlocal exchange functional combined with the Lee-Yang-Parr gradient corrected correlation functional (B3LYP).[54,55] The 6-31G (d,p) basis set was employed for all the elements. The adsorption energy (E_{ad}) for a triplet O_2 on nanotube was calculated as Equation (1):

$$E_{ad} = E_{CNT} + E_{O_2} - E_{CNT-O_2} \qquad \text{Equation (1)}$$

3. Results and discussion

We consider that C_2H_5OH can be readily decomposed into a number of carbon containing gases, such as CH_4, CO, C_2H_2 and C_2H_4 at high temperature. This will result in the different growth rate of CNTs at the same cross section level, which can deform the graphite of CNTs and introduce the curvatures containing pentagon, heptagon and octagon structures.[56] As shown in Figure 1 and S1 in Electronic Supplementary Materials, all the TCNTs samples show similar diameters of 20~30 nm with the wall thickness of 7~10 nm. Compared with straight CNTs (Figure 1g, h), TCNTs present twisted morphologies with apparent convex and concave

structures. Moreover, the nanotubes evolve from freshwater algae-like (TCNTs-1, Figure 1a, b) to bamboo-like (TCNTs-2, Figure 1c, d) and eventually to twining vine-like (TCNTs-3, Figure 1e, f) morphology. These convex and concave structures are definitely produced by the topological defects, because the only possible heteroatom oxygen doping could be excluded by the XPS analysis (S2 in Electronic Supplementary Materials).

Although any obvious diffraction changes in XRD were not witnessed (S2 in Electronic Supplementary Materials), the introduction of non-hexagon structures into CNTs could lead to the broken symmetry of graphite, and thus induce an increased D band in Raman spectra. As shown in Figure 2a, the three TCNT samples (black lines) show a much stronger D mode than the straight CNT ones (gray lines), and hence a higher ratio of D mode to G mode intensities (I_D/I_G) is obtained for TCNTs (Figure 2b). In detail, for the straight CNT samples, the ratio of I_D/I_G decreases gradually from 0.62 (CNTs-1), 0.58 (CNTs-2) to 0.43 (CNTs-3) with increasing the preparation temperature due to the improved crystallization degree of graphitic structure. In contrast, the I_D/I_G for TCNTs increases from 0.92 (TCNTs-1), 1.18 (TCNTs-2) to 1.32 (TCNTs-3), arisen from the increasing topological defect density in TCNTs. These results indicate that the CNTs with topological defects have been successfully achieved, and the topological defect density has been continuously modulated.

To reveal the effect of topological defects on the electron distribution, we performed DFT calculation on pristine and defected CNT models by the frontier molecular orbital analysis, as shown in Figure 3 (S3 in Electronic Supplementary Materials). It is found that the orbitals of the pristine CNT(5,5) delocalize and distribute uniformly over the whole surface of nanotube (Figure 3a). When one pentagon is introduced to CNT(5,5), the distribution of orbitals does not show much apparent change (PCNT(5,5), as shown in Figure 3b). Interestingly, double pentagons can

give a great disturbance to these delocalized orbitals, presented by the concentrated distribution with pentagons as center and ridge (dPCNT(5,5), Figure 3c). And this orbital evolution is the same in the case of heptagons (Figure 3d,e). The results suggest that topological defects can break the delocalization of orbitals on CNTs and promote the orbital localization, which play the same role to the heteroatom doping and may be favorable for the O_2 adsorption and dissociation in ORR process.

The electrocatalytic ORR activities of TCNT and CNT samples were first evaluated by CV in 0.1 M NaOH at a scan rate of 50 mV s^{-1} (Figure 4a). For all the CNT samples, two weak reduction peaks at around -0.32/-0.7 V are observed and the highest peak current density is only 0.55 mA cm^{-2} on CNTs-1, indicating a predominant 2-electron transfer process for the ORR.[57] With topological defects, TCNTs present a greatly enhanced activity, reflected by one sharp peak in CV curves with the highest about four fold current density (2.12 mA cm^{-2}) and a more positively shifted potential by ~ 120 mV (at about -0.2 V) compared to that of the CNTs. The peak current density noticeably increases from 1.12 (TCNTs-1), 1.35 (TCNTs-2) to 2.12 mA cm^{-2} (TCNTs-3), and the corresponding peak potential also shows a gradually positive shift from -0.22, -0.21 to -0.20 V, which indicates the strong dependence of the ORR performance on topological defect density of TCNTs. The electrocatalytic activity of TCNTs-3 was compared with commercial Pt/C in both CV and RDE voltammetries (Figure 4b, c and S5 in Electronic Supplementary Materials). In Figure 4b, it is seen that the net current density caused by the ORR on TCNTs (1.83 mA cm^{-2}) is higher by 0.19 mA cm^{-2} than that on Pt/C (1.64 mA cm^{-2}), although Pt/C catalyst has positive peak potentials as well as a higher ORR peak current density of 3.65 mA cm^{-2} than TCNTs-3 (2.12 mA cm^{-2}) based on a much stronger background current. The following RDE voltammetry shows that the steady-state diffusion current density at -0.35 V is

4.68, 4.18 and 0.98 mA cm^{-2} for TCNTs-3, Pt/C and CNTs-3 catalysts, respectively (Figure 4c). Though the present performance of TCNTs is not yet as good as the Pt/C catalyst in the peak potential, the proportional relationship between ORR performance and topological defect density suggests the great potential of TCNTs for further improvement.

RRDE voltammetries were operated to determine the transferred electron number (n) per oxygen molecule and the yield of H_2O_2 in ORR, calculated by Equation (2) and (3), respectively.[58]

$n=4I_L/(I_L+I_R/N)$ Equation (2)

$\%H_2O_2=100*(2I_R/N)/(I_L+ I_R/N)$ Equation (3)

Where I_L is the faradic disk current and I_R is the faradic ring current, and the collection efficiency N is 0.27 here. In Figure 5, n is calculated to be 2.2 (CNTs-1), 3.6 (TCNTs-1), 3.6 (TCNTs-2), 3.8 (TCNTs-3) and 3.9 (Pt/C), and the corresponding H_2O_2 yield is 92.11%, 17.1%, 16.5%, 10.4% and 8.1% at -0.35 V. These results mean that much more O_2 molecules are reduced through a 4 electron transfer process on TCNTs than on CNTs, and the O_2 reduction process based on TCNTs is similar to that on Pt/C.

To understand the electrocatalytic activity for TCNTs, O_2-stripping voltammetries were developed and performed on TCNT catalysts (Figure 6). The corresponding CV curve for TCNTs-1, TCNTs-2 and TCNTs-3 catalysts shows a single peak in the first scan (solid line), whereas the peak disappears in the second scan (dashed line). This indicated that these peaks are attributed to the dissociation of O_2 adsorbed on the catalysts. It is known that the adsorbed amount of reactant is proportional to the total charge Q consumed during the reduction of these adsorbed molecules, i.e. to the integral of the reduction current i over the potential range of reduction E_{start} (E_s) to E_{end} (E_e) according to the Equation (4):

$$Q = \int_{E_s}^{E_e} idE = nFA\Gamma$$ Equation (4)

Where n is the number of electrons in the electrode reaction, F is the Faraday constant, A is the surface area of the electrode (0.071 cm^2) and Γ is the surface concentration of the adsorbed species. Q value obtained by integration is 6.8 (TCNTs-1), 8.2 (TCNTs-2) and 10.5 μC (TCNTs-3), and the corresponding Γ is then calculated to be 2.61×10^{-10}, 3.16×10^{-10} and 4.02×10^{-10} mol cm^{-2}. Obviously, the order of Γ is consistent with the change of the topological defect density of TCNTs (Figure 3). Therefore, topological defect structure of TCNTs can facilitate the O_2 adsorption, and this provides the precondition for the subsequent O_2 dissociation, which is further understood through the theoretical calculation.

We performed DFT calculation to reveal the O_2 side-on adsorptions to CNTs and TCNTs models (Figure 7 and S6&7 in Electronic Supplementary Materials). Although the C-O bond lengths change no much (< 0.03 Å), the absolute value of O_2 binding energy (BE) decreases greatly when doping the CNT with pentagon or heptagon. For example, BE for O_2 on CNT(5,5) is -1.01 eV, which declines to -0.44 eV on PCNT(5,5) and -0.41 eV on HCNT(5,5) (the negative value indicates the unfavorable barrier to overcome when the adsorption occurs[59,60]). For dPCNT(5,5)/dHCNT(5,5), surprisingly, the O_2 adsorptions are favorable with positive BE values (0.16/0.21 eV). The energy gaps between HOMO and LUMO ($E_{HOMO-LUMO}$) of various CNT model catalysts were calculated. We find that the introduction of pentagons or heptagons shrinks the $E_{HOMO-LUMO}$ from 1.52 eV (CNT(5,5)) to 1.15 eV (dPCNT(5,5)) or even to 0.51 eV (dHCNT(5,5)), which greatly favors the reactivity of the CNTs. Therefore, CNTs with more pentagons or heptagons are more likely to activate O_2 with much lowered energy barriers to overcome for O_2 chemisorption.

The electrocatalytic stability for the electrocatalysts was investigated by the chronoamperometric responses at the same polarizing potential of -0.3 V (Figure 8). It is learnt that the currents for the three electrocatalysts of Pt/C, TCNTs-3 and CNTs-3 reach a relatively stable state after a brief transient period. The current densities follow the order of TCNTs-3>Pt/C>CNTs-3, which is consistent with the RDE results (Figure 4c). A slight deterioration of Pt occurs after a continuous 30000 s scan, while the currents for both TCNTs-3 and CNTs-3 electrodes keep almost the same level after 40000 s tests, which indicates a superior stability of TCNTs to Pt/C catalysts. These results also suggest that the introduction of topological defect structure would not destroy the stability of CNTs.

In addition to the electrocatalytic activity and long-term stability for ORR, methanol crossover and CO poisoning are another main challenge in fuel cells. The chronoamperometric responses to the methanol or CO introduced into the O_2-saturated electrolyte were performed for TCNT and Pt/C catalysts, as shown in Figure 8. After the addition of 1.0 mL methanol, the ORR current for TCNT catalyst did not show obvious change; in contrast, the ORR current for Pt/C catalyst decreased sharply and even lowed to a negative current due to the mixed potential (Figure 9a).[61] When CO with the same flow of O_2 was introduced, the ORR current for Pt/C was greatly weakened by ~25.7%, much larger than the decrease by ~11.1% for TCNTs (Figure 9b). By introducing N_2 to replace CO, the ORR current for Pt/C decreased only by ~9.9%, much smaller than ~25.7% for the case of CO, while the decrease for TCNTs kept the same level as the case of CO (~11.1%). Thus, the study results proved that the great current decrease for Pt/C mainly resulted from the CO poisoning, while the small one for TCNTs from the decreased solubility of O_2 in the electrolyte due to the decreased partial pressure of O_2 (Henry's Law).[62,63] This indicates

that Pt/C catalyst is sensitive to methanol and CO poisoning, while TCNTs maintain a high stability and immunity.

4. Conclusions

A new kind of metal-free electrocatalysts of pristine CNTs with topological defects have been developed that exhibit quite a good performance for the ORR in electrocatalytic activity, stability, and immunity towards methanol crossover and CO poisoning. The electrocatalytic performances are improved progressively with increasing topological defect density, as reflected by the increasing reduction current density and the positively shifted peak potentials. The good performance of the TCNT catalysts mainly come from i) the introduction of topological defect breaks the delocalization of orbital and promotes the formation of localized orbital on CNTs; ii) the localized orbital is favorable for the O_2 adsorption and the subsequent O_2 dissociation. This work suggests that apart from doping heteroatom into CNTs, tuning the surface structure of CNTs with non-hexagon carbon structure is a novel and efficient way for exploring advanced metal-free ORR electrocatalysts.

Acknowledgements

We gratefully acknowledge the support from the National Natural Science Foundation of China (21103019, 21307011 and 21303271), the Foundation of Key Laboratory of Radioactive Geology and Exploration Technology Fundamental Science for National Defense (RGET1214 and RGET1312) and the Start-up Fund of the East China Institute of Technology (DHBK1005 and DHBK1009).

References

1. H. A. Gasteiger, N. M. Markovic, *Science*, 2009, **324**, 48-49.
2. M. Winter, R. J. Brodd, *Chem. Rev.*, 2004, **104**, 4245-4269.
3. M. K. Debe, *Nature*, 2012, **486**, 43-51.
4. www.platinum.matthey.com/pgm-prices/price-charts (accessed Aug 17, 2014).
5. J. Zhang, K. Sasaki, E. Sutter, R. R. Adzic, *Science*, 2007, **315**, 220-224.
6. C. Wang, H. Daimon, Y. M. Lee, J. Kim, S. H. Sun, *J. Am. Chem. Soc.*, 2007, **129**, 6974-6975.
7. V. Stamenkovic, B. S. Mun, K. J. J. Mayrhofer, P. N. Ross, N. M. Markovic, J. Rossmeisl, J. Greeley, J. K. Nørskov, *Angew. Chem. Int. Ed.*, 2006, **45**, 2897-2901.
8. N. Tian, Z. Y. Zhou, S. G. Sun, Y. Ding, Z. L. Wang, *Science*, 2007, **316**, 732-735.
9. C. Wang, D. Vliet, K. L. More, N. J. Zaluzec, S. Peng, S. H. Sun, H. Daimon, G. F. Wang, J. Greeley, J. Pearson, A. P. Paulikas, G. Karapetrov, D. Strmcnik, N. M. Markovic, V. R. Stamenkovic, *Nano Lett.*, 2011, **11**, 919-926.
10. V. Mazumder, M. F. Chi, K. L. More, S. H. Sun, *J. Am. Chem. Soc.*, 2010, **132**, 7848-7849.
11. S. J. Jiang, Y. W. Ma, G. Q. Jian, H. S. Tao, X. Z. Wang, Y. N. Fan, Y. N. Lu, Z. Hu, Y. Chen, *Adv. Mater.*, 2009, **21**, 4953-4956.
12. C. L. Zhang, S. Y. Hwang, A. Trout, Z. M. Peng, *J. Am. Chem. Soc.*, 2014, **136**, 7805-7808.
13. K. Uosaki, G. Elumalai, H. Noguchi, T. Masuda, A. Lyalin, A. Nakayama, T. Taketsugu, *J. Am. Chem. Soc.*, 2014, **136**, 6542-6545.
14. Y. Y. Liang, Y. G. Li, H. L. Wang, J. G. Zhou, J. Wang, T. Regier, H. J. Dai, *Nat. Mater.*, 2011, **10,** 780-786.
15. Z. Yang, X. M. Zhou, Z. P. Jin, Z. Liu, H. G. Nie, X. A. Chen, S. M. Huang, *Adv. Mater.*, 2014, **26**, 3156-3161.
16. G. Wu, K. L. More, C. M. Johnston, P. Zelenay, *Science*, 2011, **332**, 443-447.
17. H. Y. Zhu, S. Zhang, Y. X. Huang, L. H. Wu, S. H. Sun, *Nano Lett*., 2013, **13**, 2947-2951.
18. D. H. Deng, L. Yu, X. Q. Chen, G. X. Wang, L. Jin, X. L. Pan, J. Deng, G. Q. Sun, X. H. Bao, *Angew. Chem. Int. Ed.*, 2013, **125**, 389-393.
19. G. Tuci, C. Zafferoni, A. Rossin, A. Milella, L. Luconi, M. Innocenti, L. T. Phuoc, C. Duong-Viet, C. Pham-Huu, G. Giambastiani, *Chem. Mater.*, 2014, **26**, 3460-3470.

20. R. Ning, J. Q. Tian, A. M. Asiri, A. H. Qusti, A. O. Al-Youbi, X. P. Sun, *Langmuir* 2013, **29**, 13146.
21. 20. S. Mao, Z. H. Wen, T. Z. Huang, Y. Hou, J. H. Chen, Energy Environ. Sci. 2014, 7, 609-616.
22. 21. A. Morozan, B. Jousselme, S. Palacin, *Energy Environ. Sci.*, 2011, 4, 1238-1254.
23. 22. M. Li, X. J. Bo, Y. F. Zhang, C. Han, A. Nsabimana, L. P. Guo, *J. Mater. Chem. A*, 2014, 2, 11672-11682.
24. 23. D. D. Wang, X. Chen, D. G. Evans, W. S. Yang, *Nanoscale*, 2013, 5, 5312-5315.
25. K. P. Gong, F. Du, Z. H. Xia, M. Durstock, L. M. Dai, *Science*, 2009, **323**, 760-764.
26. L. T. Qu, Y. Liu, J. B. Baek, L. M. Dai, *ACS Nano*, 2010, **4**, 1321-1326.
27. Z. Liu, H. G. Nie, Z. Yang, Z. P. Jin, Y. Q. Liu, Z. B. Xiao, S. M. Huang, *Nanoscale*, 2013, 5, 3283-3288.
28. R. L. Liu, D. Q. Wu, X. L. Feng, K. Mullen, *Angew. Chem. Int. Ed.*, 2010, **49**, 2565-2569.
29. Z. W. Liu, F. Peng, H. J. Wang, H. Yu, W. X. Zheng, J. Yang, *Angew. Chem. Int. Ed.*, 2011, **50**, 3257-3261.
30. Y. Zheng, Y. Jiao, J. Chen, J. Liu, J. Liang, A. Du, W. Zhang, Z. Zhu, S. C. Smith, M. Jaroniec, G. Q. Lu,; S. Z. Qiao, *J. Am. Chem. Soc.*, 2011, **133**, 20116-20119.
31. J. Liang, Y. Zheng, J. Chen, J. Liu, D. Hulicova-Jurcakova, M. Jaroniec, S. Z. Qiao, *Angew. Chem. Int. Ed.*, 2012, **51**, 3892-3896.
32. S. B. Yang, X. L. Feng, X. C. Wang, K. Mullen, *Angew. Chem. Int. Ed.*, 2011, **50**, 5339 - 5343.
33. J. Y. Cheon, J. H. Kim, K. C. Goddeti, J. Y. Park, S. H. Joo, *J. Am. Chem. Soc.*, 2014, **136**, 8875-8878.
34. T. Xing, Y. Zheng, L. H. Li, B. C. C. Cowie, D. Gunzelmann, S. Z. Qiao, S. M. Huang, Y. Chen, *ACS Nano*, 2014, **8**, 6856-6862.
35. J. T. Jin, F. P. Pan, L. H. Jiang, X. G. Fu, A. M. Liang, Z. Y. Wei, J. Y. Zhang, G. Q. Sun,. *ACS Nano*, 2014, **8**, 3313-3321.
36. H. W. Liang, Z. S. Wu, X. L. Feng, K. Mullen, J. Am. Chem. Soc. 2013, **135**, 16002-16005.
37. Q. Liu, J. Y. Zhang, *Langmuir*, 2013, **29**, 3821-3828.
38. Z. Yang, Z. Yao, G. F. Li, G. Y. Fang, H. G. Nie, Z. Liu, X. M. Zhou, X. A. Chen, S. M. Huang, *ACS Nano*, 2012, **6**, 205-211.

39. D. S. Yang, D. Bhattacharjya, S. Inamdar, J. Park, J. S. Yu, *J. Am. Chem. Soc.*, 2012, **134**, 16127-16130.
40. L. J. Yang, S. J. Jiang, Y. Zhao, L. Zhu, S. Chen, X. Z. Wang, Q. Wu, J. Ma, Y. W. Ma, Z. Hu, *Angew. Chem. Int. Ed.*, 2011, **50**, 7132-7135.
41. D. W. Wang, D. S. Su, *Energy Environ. Sci.*, 2014, 7, 576-591.
42. R. Ning, C. J. Ge, J. Q. Tian, A. M. Asiri, K. A. Alamry, C. M. Li, X. P. Sun, *Carbon* 2014, **78**, 60-69.
43. J. Q. Tian, R. Ning, Q. Liu, A. M. Asiri, A. O. Al-Youbi, X. P. Sun, *ACS Appl. Mater. Interfaces* 2014, **6**, 1011-1017.
44. Y. J .Tian, Z. Hu, Y. Yang, X. Z. Wang, X. Chen, H. Xu, Q. Wu, W. J. Ji, Y. Chen, *J. Am. Chem. Soc.*, 2004, **126**, 1180-1183.
45. T. Lenosky, X. Gonze, M. Teter, V. Elser, *Nature*, 1992, **355**, 333-335.
46. H. F. Bettinger, *J. Phys. Chem. C*, 2005, **109**, 6922-6924.
47. S. Iijima, T. Ichihashi, Y. Ando, *Nature*, 1992, **356**, 776-778.
48. J. C. Charlier, T. W. Ebbesen, Ph. Lambin, *Phys. Rev. B*, 1996, **53**, 11108-11113.
49. T. W. Ebbesen, T. Takada, *Carbon*, 1995, **33**, 973-978.
50. J. C. Charlier, *Acc. Chem. Res.*, 2002, **35**, 1063-1069.
51. L. Rincon, R. Almeida, C. A. Gonzalez, *J. Phys. Chem. C*, 2011, **115,** 11727-11733.
52. S. J. Lee, H. J. Kim, J .Lee, Y. Kuk, K. H. Chung, H. Kim, S. J. Kahng, *Surface Science*, 2006, **600**, 4937-4940.
53. M. J. Frisch, et al. Gaussian 09, Revision A.02; Gaussian, Inc.: Wallingford, CT, **2009**. (S8 in Electronic Supplementary Materials).
54. A. D. Becke, *J. Chem. Phys.*, 1993, **98**, 5648-5652.
55. P. J. Stephens, F. J. Devlin, C. F. Chabalowski, M. J. Frishch, *J. Phys. Chem.*, 1994, **98**, 11623-11627.
56. S. Amelinckx, X. B. Zhang, D. Bernaerts, X. F. Zhang, V. Ivanov, J. B. Nagy, *Science*, 1994, **29**, 635-639.
57. X. Xu, S. J. Jiang, Z. Hu, S. Q. Liu, *ACS Nano*, 2010, **4,** 4292-4298.
58. S. T. Chang, C. H. Wang, H. Y. Du, H. C. Hsu, C. M. Kang, C. C. Chen, J. C. S. Wu, S. C. Yen, W. F. Huang, L. C. Chen, M. C. Lin, K. H. Chen, *Energy Environ. Sci.*, 2012, **5**, 5305-5314.

59. X. B. Hu, Y. T. Wu, H. R. Li, Z. B. Zhang, *J. Phys. Chem. C*, 2010, **114**, 9603-9607.
60. P. Giannozzi, R. Car, G. Scoles, *J. Chem. Phys.*, 2003, **118**, 1003-1006.
61. V. A. Paganin, E. Sitta, T. Iwasita, W. J. Vielstich, *J. Appl. Electrochem.*, 2005, **35**, 1239-1243.
62. R. F. Mann, J. C. Amphlett, B. A. Peppley, C. P. Thurgood, *J. Power Sources*, 2006, **161**, 768-774.
63. V. A. Sethuraman, S. Khan, J. S. Jur, A. T. Haug, J.W. Weidner, *Electrochim. Acta*, 2009, **54**, 6850-6860.

Figures and Captions

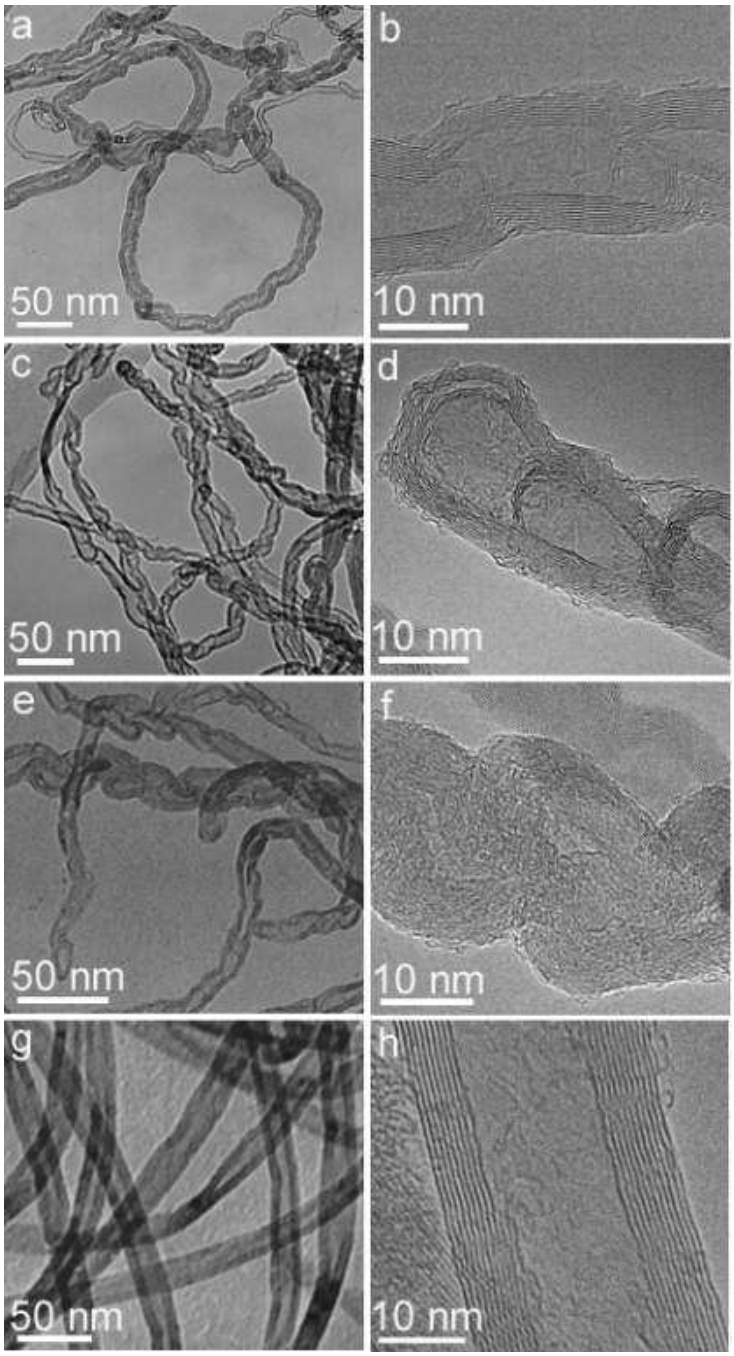

Figure 1. TEM (a, c, e, g) and HRTEM (b, d, f, h) images of TCNTs and CNTs. TCNTs-1 (a,b), TCNTs-2 (c,d), TCNTs-3 (e,f) and CNTs-3 (g,h).

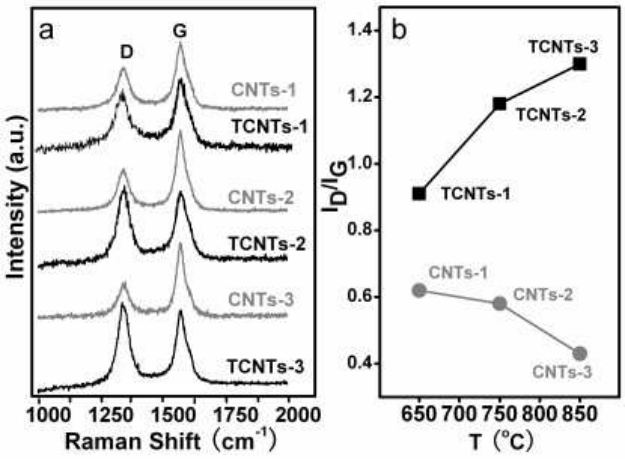

Figure 2. Raman spectra and derived parameters. (a) Raman spectra for CNTs (gray lines) and TCNTs (black lines). (b) The derived profile of I_D/I_G versus the preparation temperature.

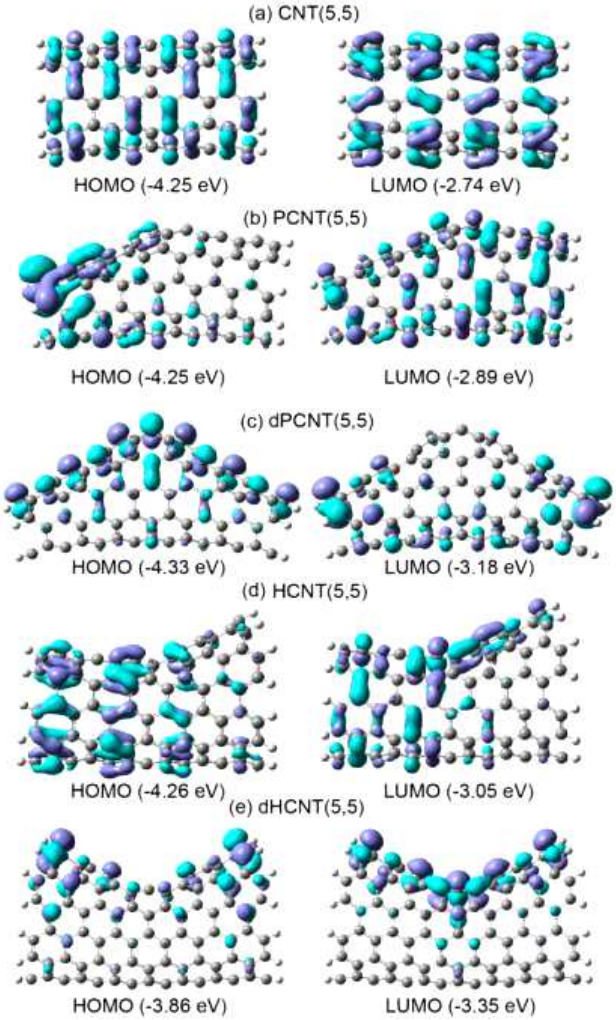

Figure 3. The highest occupied molecular orbital (HOMO) and the lowest unoccupied molecular orbital (LUMO) plots of (a) the pristine CNT(5,5), (b,c) single or double pentagon(s)-doped CNT(5,5) (PCNT(5,5), dPCNT(5,5)), and (d,e) single or double heptagon(s)-doped CNT(5,5) (HCNT(5,5), dHCNT(5,5)) with their eigenvalues.

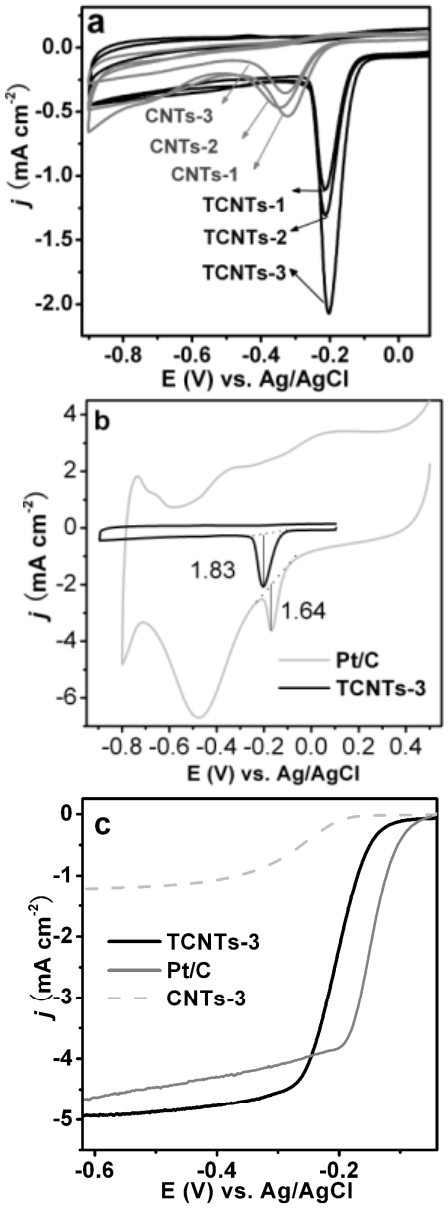

Figure 4. Electrocatalytic tests of PCNT, CNT and Pt/C catalysts for the ORR in O_2-saturated 0.1 M NaOH electrolyte. (a,b) CV curves (scan rate 50 mV s^{-1}). (c) RDE voltammetry with a rotation speed of 2500 rpm (scan rate 10 mV s^{-1}).

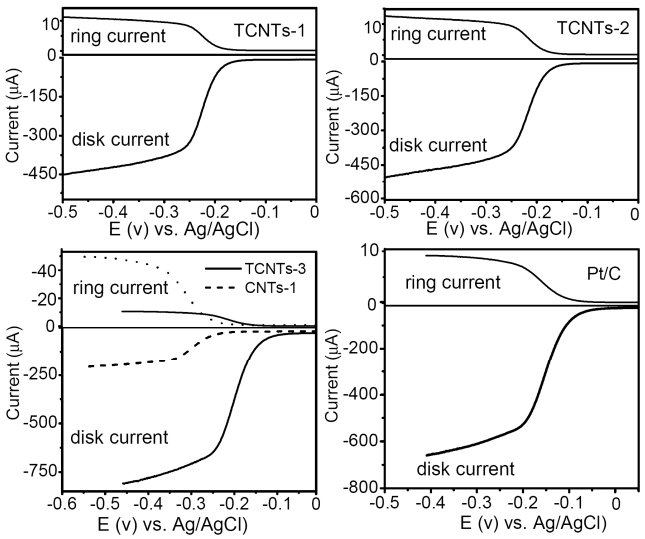

Figure 5. RRDE voltammetries of ORR for TCNTs, CNTs and Pt/C in O_2-saturated 0.1 M NaOH electrolyte at a rotation rate of 2000 rpm and a scan rate of 5 mV s^{-1}. During the tests, Pt ring electrode is polarized at 0.5 V.

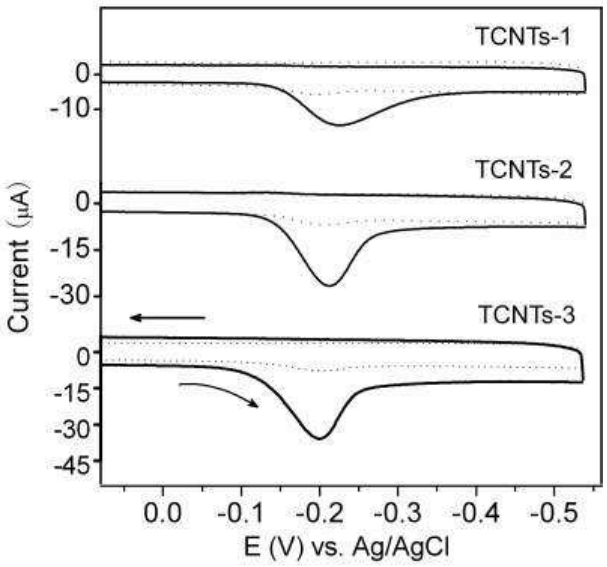

Figure 6. O_2-stripping voltammetry curves for TCNTs-1, TCNTs-2 and TCNTs-3 catalysts in 0.1 M NaOH with a scan rate of 5 mV s^{-1}.

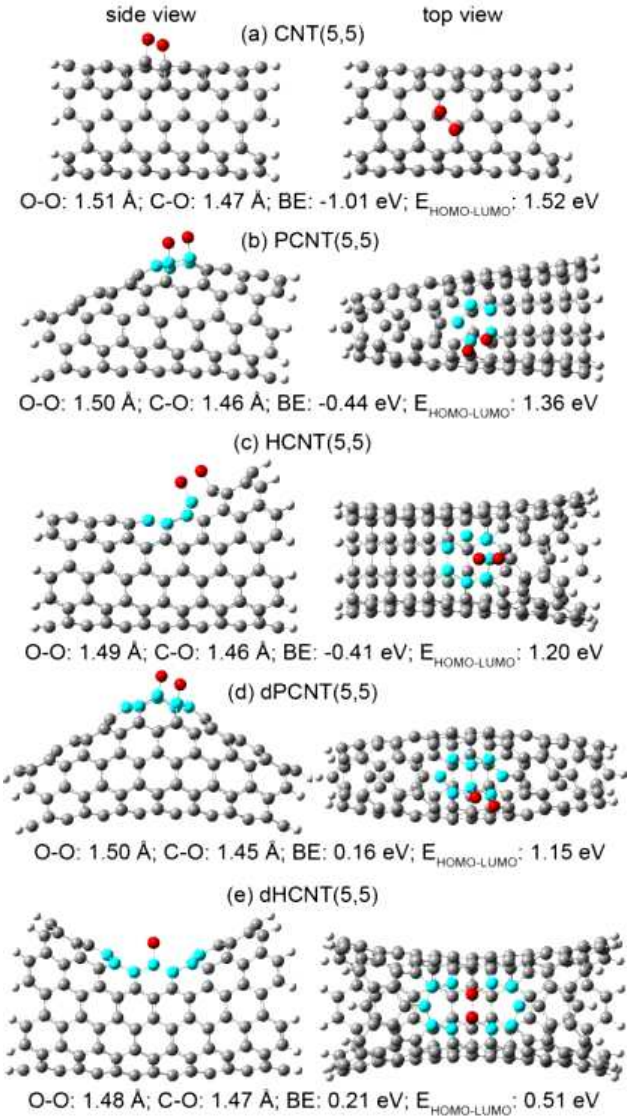

Figure 7. The most stable structures and the corresponding parameters for O_2 adsorption on (a) CNT(5,5), (b) PCNT(5,5), (c) HCNT(5,5), (d) dPCNT(5,5), and (e) dHCNT(5,5).

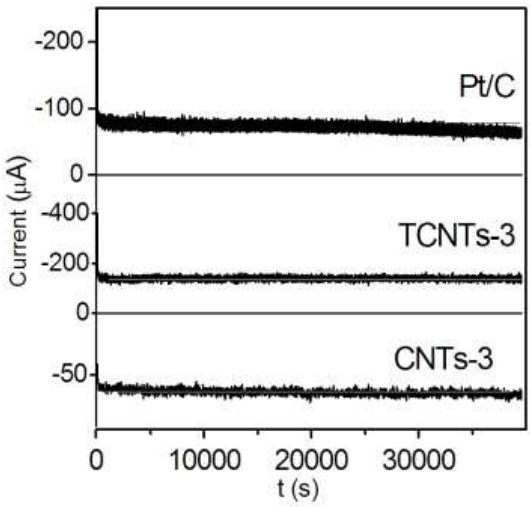

Figure 8. The steady-state chronoamperometric response at the polarizing potential of -0.3 V in the O_2-saturated electrolyte for TCNTs-3, CNTs-3 and Pt/C catalysts. The dotted lines are given as horizontal reference to investigate the changes of current signals.

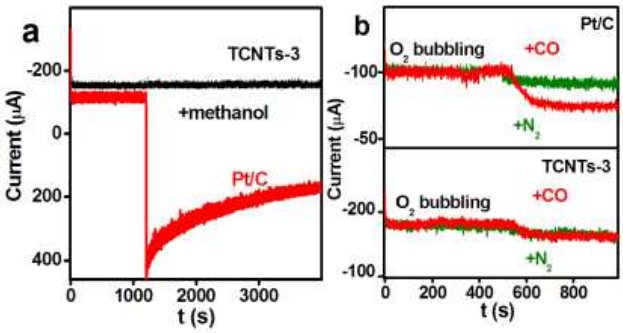

Figure 9. The steady-state chronoamperometric responses in the O_2-saturated electrolyte for TCNTs-3 and Pt/C (20 wt% Pt loading) catalysts. (a) Methanol crossover tests by introducing 1.0 mL methanol into the electrolyte at 1200 s. (b) CO poisoning tests by introducing additional 50 V% CO into the electrolyte at 520 s (red). Parallel experiments for TCNTs-3 and Pt/C catalysts are carried out by replacing CO with N_2 (green).